

Article

Facile and Eco-Friendly Preparation of Mild Steel Based Superhydrophobic Surfaces without Chemical Modifications

Wenxuan Jiang ¹, Yujun Liu ¹, Ji Wang ^{1,2,3,*}, Rui Li ¹, Xiao Liu ¹ and Shaohua Ai ¹

¹ School of Naval Architecture and Ocean Engineering, Dalian University of Technology, No.2 Linggong Road, Ganjingzi District, Dalian 116024, China; jwx_thealpha@foxmail.com (W.J.); yjliu@dlut.edu.cn (Y.L.); lirui@dlut.edu.cn (R.L.); liuxiao@dlut.edu.cn (X.L.); aaishaohua@163.com (S.A.)

² Collaborative Innovation Centre for Advanced Ship and Deep-Sea Exploration, Shanghai Jiaotong University, No. 800 Dongchuan Road, Minhang District, Shanghai 200240, China

³ State Key Laboratory of Structural Analysis for Industrial Equipment, Dalian University of Technology, Dalian 116024, China

* Correspondence: wangji@dlut.edu.cn

Abstract: The fabrication of superhydrophobic coatings on mild steel has attracted considerable attention. However, some methods are cumbersome and unsuitable for large-scale preparation, limiting industrial applications. Furthermore, the extensive use of fluorinated compounds to achieve low surface energy is not environmentally friendly. This paper proposed a facile method based on electrodeposition and annealing to prepare mild steel-based superhydrophobic surfaces without chemical modifications. Subsequently, SEM images were analyzed, and it was observed that the plating parameter (current and time) significantly affected surface morphology. At optimum process parameters, a rough surface with a multi-level structure was formed on the plated surface, contributing to superhydrophobic properties. XPS, EDS, and XRD were utilized to analyze surface composition. The results indicated the presence of copper oxides, zinc oxides, and a large number of hydrocarbons on the prepared superhydrophobic surface. These transition metal oxides on the surface adsorbed hydrocarbons in the air during the annealing process, which lowered the surface energy. Combined with the obtained multi-level morphology, a superhydrophobic surface was achieved. Finally, the corrosion behavior was evaluated in 3.5 wt% NaCl solution by AC impedance spectroscopy. Results showed that the obtained superhydrophobic surface, compared with the untreated coating and the steel substrate, showed a substantial improvement in corrosion resistance. A mild steel-based superhydrophobic surface with a contact angle greater than 150 degrees and excellent corrosion resistance was finally obtained. We hope this study will facilitate the industrial preparation of superhydrophobic coatings, especially in marine engineering, since this method does not require complex processes or expensive equipment and does not require fluorinated substances.

Keywords: mild steel substrate; superhydrophobic surface; eco-friendly; process parameters; corrosion resistance; electrodeposition; eco-friendly



Citation: Jiang, W.; Liu, Y.; Wang, J.; Li, R.; Liu, X.; Ai, S. Facile and Eco-Friendly Preparation of Mild Steel Based Superhydrophobic Surfaces without Chemical Modifications. *Coatings* **2022**, *12*, 737. <https://doi.org/10.3390/coatings12060737>

Academic Editor: Fabio Palumbo

Received: 28 April 2022

Accepted: 25 May 2022

Published: 27 May 2022

Publisher's Note: MDPI stays neutral with regard to jurisdictional claims in published maps and institutional affiliations.



Copyright: © 2022 by the authors. Licensee MDPI, Basel, Switzerland. This article is an open access article distributed under the terms and conditions of the Creative Commons Attribution (CC BY) license (<https://creativecommons.org/licenses/by/4.0/>).

1. Introduction

Mild steel is widely used in industrial and engineering construction, especially in marine engineering, because of its high specific strength, weldability, machinability, and low cost [1–4]. However, mild steel is prone to corrosion when exposed to humid working environments, resulting in substantial economic losses and safety accidents. Three means have been developed to protect mild steel from corrosion, including cathodic protection, anodic protection [5], and the application of barrier coatings [6]. Among all coatings, superhydrophobic coatings are the most effective method to prevent mild steel from contact with corrosive environments. Moreover, the preparation of mild steel-based superhydrophobic surfaces has become a hot research topic in recent years [7–9].

Superhydrophobic surfaces are mainly achieved by associating micro/nanoscale rough surfaces and low surface energy materials [10,11]. Numerous methods have been used to prepare mild steel-based superhydrophobic surfaces, including spraying [12,13], IR laser [14,15], etching [16–18], sol–gel [19–21], electrodeposition [22], hot-dip plating [23], plasma sputtering [24], etc. However, considering the practical application requirements for metal protection, some critical issues of superhydrophobic coatings still need to be addressed. Current technologies still have several limits in the large-scale manufacture and practical applications, such as rigorous experimental conditions and complex preparatory procedures.

It is well known that the electrochemical deposition process is simple to implement and does not require any special equipment or harsh conditions. This method has been frequently utilized to investigate superhydrophobic coatings based on mild steel. In general, there are two types of electrodeposition preparation methods. One is “morphology + modification”: Electrodeposition was used to create micro/nano morphology, which was then chemically modified [25,26]. Typically, the modification is carried out in an ethanolic solution of tetradecanoic acid, stearic acid, or other fluorinated compounds [27,28]. Hu et al. [29] prepared a titanium dioxide and zinc composite coating (modified by stearic acid) on the surface of carbon steel with good hydrophobicity and stability. Tian et al. [30] prepared a novel superhydrophobic Zn-Fe alloy coating on the surface of carbon steel. The electroplated surface was modified by tetradecanoic acid to obtain superhydrophobicity.

The other category is a one-step electrodeposition method to obtain the surface directly [31,32]. This method is usually performed in an ethanol electrolyte to deposit chemical compounds (usually formed by low surface energy substances and metal cations) onto the cathode surface. Heidari et al. [33] prepared a superhydrophobic surface by one-step electrodeposition on a carbon steel surface to enhance the surface’s corrosion resistance. The superhydrophobic surface was composed of $\gamma\text{-Fe}_2\text{O}_3$ and $\text{Fe}(\text{CH}_3(\text{CH}_2)_{12}\text{COO})$ compositions.

When applied to large-area superhydrophobic surface preparation, these two methods are problematic. In the “morphology + modification” method, surface chemical modification requires large amounts of anhydrous ethanol, stearic acid, and even fluorinated compounds. For the preparation of large areas, this method is not controllable, has poor safety, and is not environmentally friendly. In the “One Step” method, ethanol electrolyte was utilized in the electrodeposition process, which is uncontrollable and poorly secured, considering that large plates require large amounts of anhydrous ethanol. In addition to these, nanoparticles are added to the plating solution in some studies [34]. In order to maintain a uniform dispersion of nanoparticles and avoid agglomeration, large stirring devices (such as ultrasonic generators) and significant additions of surfactants are required. Therefore, the development of simple, safe, fluorine-free, no-particles, and eco-friendly mild steel-based superhydrophobic coatings is of particular interest for industrial applications.

Previous reports mentioned metals such as copper and zinc that adsorb hydrocarbons in the air to lower surface energy and create a superhydrophobic surface [35–37]. However, few studies report this application on mild steel surfaces. Therefore, this study proposes a method based on the Cu-Zn composite electrodeposition and annealing processes to prepare mild steel-based superhydrophobic surfaces. The electrodeposition process is carried out at room temperature and does not require nanoparticles, anhydrous ethanol, various types of compounds used for surface modification or any fluorine-containing compounds. There are only two steps in the surface preparation process: one to obtain a specific roughness by electrodeposition and one to anneal the surface. Subsequently, the effect of plating parameters on surface morphology and wettability was investigated. The causes of surface hydrophobicity were also analyzed and combined with surface composition testing. Finally, the corrosion resistance of the surface was investigated by comparing the coating to the mild steel substrate.

2. Materials and Methods

2.1. Materials

Chemical reagents were of analytical grade. The mild steel plates and copper plate were obtained from Quanfu Metal Co., Ltd. (Shenzhen City, China). $\text{CuSO}_4 \cdot 5\text{H}_2\text{O}$ and $\text{ZnSO}_4 \cdot 7\text{H}_2\text{O}$ were bought from Tianli Co., Ltd. (Tianjin City, China). NaOH was purchased from Bodi Co., Ltd. (Tianjin City, China), and $\text{C}_4\text{O}_6\text{H}_4\text{KNa} \cdot 4\text{H}_2\text{O}$ was purchased from Guangfu Technology Development Co., Ltd. (Tianjin City, China).

2.2. Preparation Process

Plating conditions and specific processing parameters are listed in Table 1, and the schematic diagram of the preparation process is shown in Figure 1. In the experiment, the copper plate (60 mm × 80 mm × 5 mm) was used as the anode, and the actual immersed area was about 60 mm × 60 mm. A Q235 carbon steel (primary composition carbon C: ≤0.22%; silicon Si: ≤0.35%; manganese Mn: ≤1.4%; sulfur S: ≤0.050%; phosphorus p: ≤0.045%) sheet was used as the cathode electrode (40 mm × 60 mm × 1 mm), and the actual immersed area of the cathode is 40 mm × 40 mm. The Q235 steel plates were polished using 800, 1200, and 2000 grit size SiC sandpaper. The polished Q235 plate's contact angle is 67°. The polished plate was then pickled with acid to remove rust spots, followed by hot alkali degreasing and weak acid activation. Steel plates must be thoroughly cleaned with deionized water between all pre-treatment steps. After completing the above steps, the surface was cleaned for the last time and prepared for plating.

Table 1. Plating conditions and specific processing parameters.

Item	Parameter	Unit
Anode (Copper)	60 × 80 × 5	mm
Cathode (Mild steel)	40 × 60 × 1	mm
Current density	3, 4, 5, 6	A/dm ²
Time	30, 60, 90	min
Power supply mode	Constant current	
Plating temperature	Ambient temperature	
Annealing temperature	200	°C

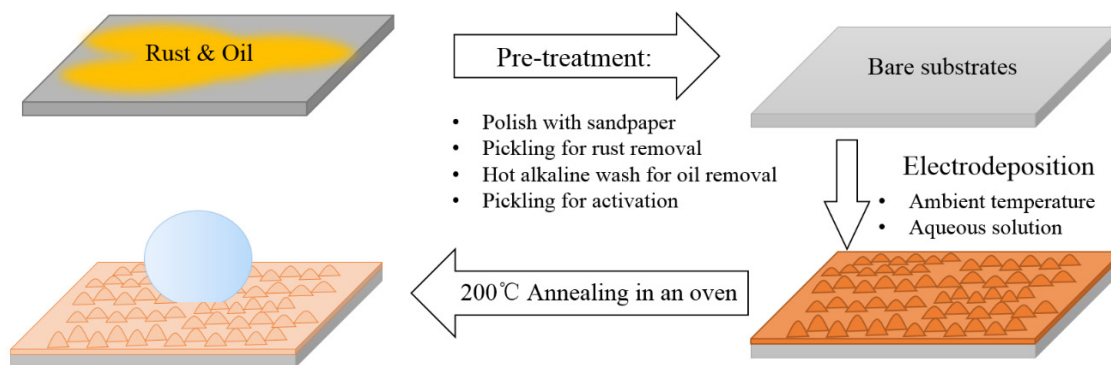


Figure 1. Mild steel-based superhydrophobic surface preparation process diagram.

The bath composition included copper sulfate pentahydrate (20 g/L), zinc sulfate heptahydrate (23 g/L), potassium sodium tartrate tetrahydrate (100 g/L), and sodium hydroxide (50 g/L) [37]. The deposition process was performed in a two-electrode cell using a digital regulated DC (direct current) power supply at ambient temperature. In order to determine the range of experimental parameters, a preliminary test was conducted. According to the test, the current density ranged from 3 A/dm² to 6 A/dm² (0.48 A~0.96 A), and the deposition time ranged from 30 min to 90 min. After the electrodeposition process, the prepared steel plates were cleaned with flowing distilled water several times and

dried with a hairdryer. These samples were then annealed in an electric oven preheated to 200 degrees C and annealed for a specified period. Afterward, the samples were stored in a closed dry sample box for one day.

2.3. Characterization

2.3.1. Morphological Characterization

A scanning electron microscope (SEM, FEI QUANTA 45003040702) was used to examine the morphologies of electroplated coatings. Samples were cut into 40 mm × 20 mm for characterization. All samples were characterized on the same scale.

2.3.2. Surface Composition Characterization

X-ray diffraction (XRD, D/Max 240003030502) was used to investigate crystal structure. Energy-disperse spectroscopy (EDS, FEI QUANTA 45003040702) and X-ray photoelectron spectroscopy (XPS, Escalab 250Xi, Thermo) were used to confirm the type and form of the coating's elements.

2.3.3. Wettability Characterization

The contact angle was measured using contact angle measurement. This contact angle measuring instrument includes a high-speed camera, liquid inlet tube, etc. The experimental droplet size is five microliters. It is necessary to wait for 2 min after droplet formation to ensure a stable droplet shape before measurement. The contact angle was measured and calculated by the goniometric method. The average value of all the measuring points for each specimen was utilized as the final contact angle.

2.3.4. Electrochemical Analysis

The electrochemical corrosion behavior was measured at 3.5 wt. % aqueous sodium chloride solution at room temperature using an electronic electrochemical workstation (CHI 660E, CH Instruments Inc., Bee Cave, TX, USA). The workstation was equipped with a standard three-electrode system. A platinum electrode was used as a counter electrode, a saturated calomel electrode (SCE), and the prepared sample was used as a reference electrode and the working electrode, respectively. In electrochemical experiments, the exposed surface of the sample in NaCl solution is a 1 cm circle in diameter. Before the electrochemical experiments, the samples' exposed areas were immersed in NaCl solution for 1000 s to achieve a stable open circuit potential (OCP). Electrochemical impedance spectroscopy (EIS) measurements were performed in the frequency range of 100 kHz–0.01 Hz with a voltage amplitude of 0.005 V.

3. Results and Discussion

3.1. To Determine the Annealing Time Parameters

In this study, annealing is an important reason for the formation of superhydrophobicity in a limited time. To determine the appropriate time for annealing, we selected electroplated samples under 60 min and the current densities of 3–6 A/dm². These samples were annealed at a series of time parameters, respectively, and then stored hermetically at room temperature. The results obtained are shown in Figure 2. For samples prepared at different current densities, the surface contact angle increased with increasing heating time.

From Figure 2, the increasing rates of contact angles were found to decrease with increasing time. Furthermore, the magnitude of the contact angle change with increasing annealing time varied between samples prepared with different parameters. This is because, for a sample, even if the contact angle increases due to the decrease in surface energy, it is necessarily limited by surface morphology (the analysis of morphology will be discussed in the next section).

For the present process, 200 degrees Celsius for 8 h is optimal for achieving superhydrophobic properties.

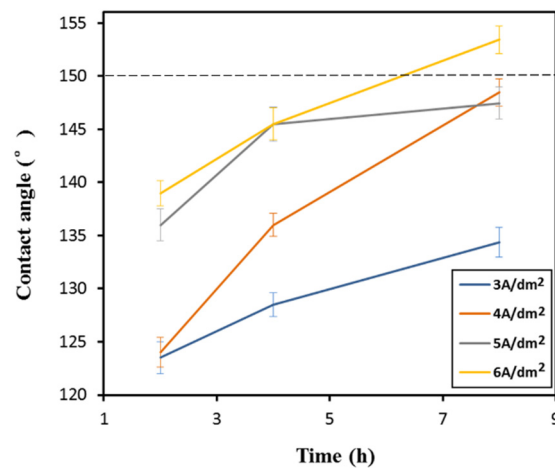


Figure 2. Annealing time-contact angle curves of samples prepared with different plating parameters.

3.2. Morphology Analysis

In comparison to other process methods, electrodeposition provides a viable method to manipulate the growth of the microstructure simply by varying electrochemical parameters such as deposition time and current density [38]. Furthermore, surface morphology is one of the two critical causes of the superhydrophobic phenomenon. In this study, the plating process was carried out under a set of current density and time parameters. In order to investigate the effect of plating parameters on surface morphology, SEM was utilized, as shown in Figure 3.

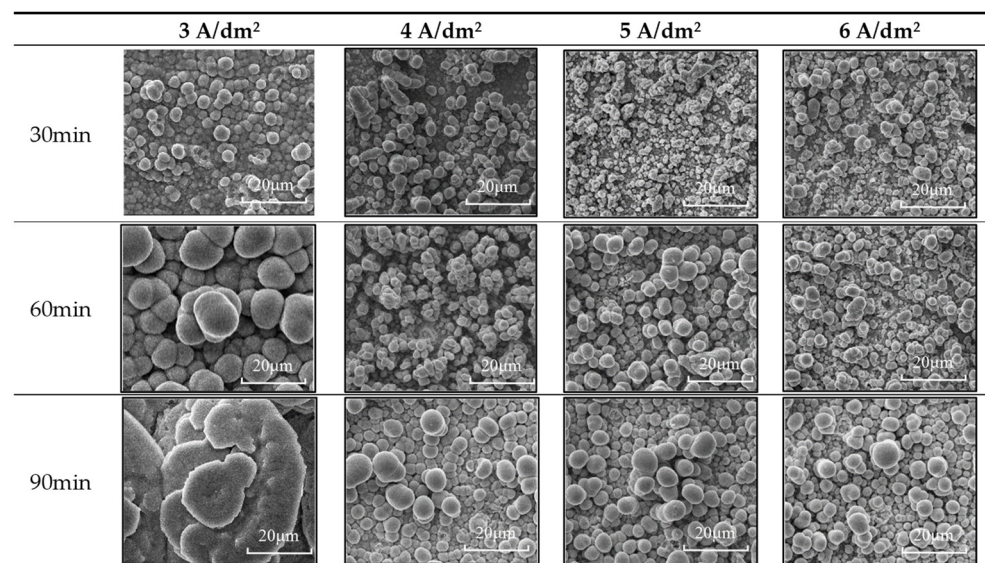


Figure 3. SEM images of samples were obtained with currents of 3–6 A/dm² and times of 30 min, 60 min, and 90 min. The scale bar is 20 μm.

Figure 3 shows SEM pictures of the prepared surface, which appears to be organized by multiple micro/nanoscale protrusions. However, the arrangement is not same. Under the same current density, the individual size of the protrusions grows with time, indicating increased “crowding.” Under the same time parameter, the number of protrusions per unit area increases, implying that an increase in current densities leads to an increase in protrusion distribution density.

These morphology changes were primarily caused by electrochemical reactions between the solution and the cathode plate. The number of free Zn²⁺ and Cu²⁺ was reduced due to the complexes formed by Zn²⁺/NaOH and Cu²⁺/C₄O₆H₄KNa (as shown

in Figure 4). Therefore, displacement reactions in the solution prior to the plating process were avoided. However, this increases the difficulty of reducing these two ions on the cathode surface, especially at high plating currents, which may trigger side reactions, such as the hydrogen precipitation reaction. H^+ is reduced on the cathode surface and forms OH^- nearby, which reacts with free Cu^{2+} and Zn^{2+} to produce a loose porous deposit consisting of $Zn(OH)_2$ and $Cu(OH)_2$. On the one hand, this non-conductive loose porous deposit increases the polarization of the steel plate; on the other hand, these microparticles of hydroxide are deposited on the cathode's surface with the reduced metal cations [39]. Both can lead to the creation of this rough surface.

In addition, large current densities cause electrochemical polarization on the cathode's surface. The increased current density promotes polarization and leads to more growth points on the surface, increasing the number of protrusions per unit area [40]. In terms of the time parameter, as deposition time increases, more metal cations are deposited on the cathode surface after a reduction at the growth points, resulting in larger protrusions [40].

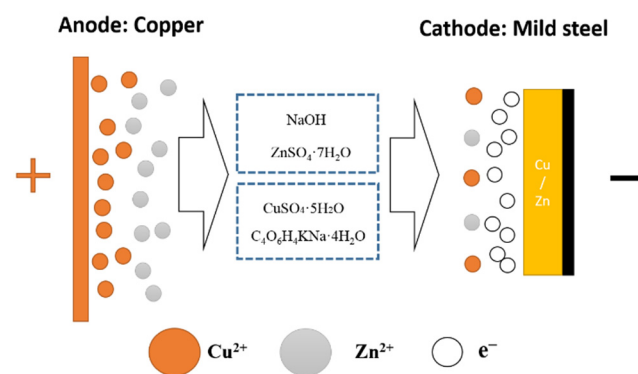


Figure 4. The free Cu^{2+} and Zn^{2+} in the solution form a complex with NaOH and $C_4O_6H_4KNa$, resulting in fewer metal cations discharging at the cathode and increasing cathodic polarization.

3.3. Surface Wettability Analysis

Figure 5 depicts the variation of the contact angle (CA) of the plated surface at various deposition times. The curves illustrate that as deposition time increases, various trends emerge at varying current densities. Samples under $3 A/dm^2$ exhibit a declining and then increasing trend; samples under $4 A/dm^2$ exhibit a gradually growing trend; samples under $5 A/dm^2$ exhibit a steady decrease, and samples under $6 A/dm^2$ exhibit an increasing and then decreasing trend. When combined with the above morphological analysis, we discover that the surface contact angle does not increase with protrusion growth; and different current densities result in varied protrusion distributions. The impact of increasing the size of individual protrusions varies with protrusion distribution density. Therefore, the time parameter must be matched with the current density in order to obtain proper morphology. Figure 6 depicts the variation of the contact angle (CA) corresponding to different deposit current densities. The curves show that the CA (contact angle) values tend to increase as the deposition current density increases. We discussed in the previous morphological analysis how high current densities promote electrochemical polarisation, resulting in increased protrusion distribution density. The increased protrusion densities provide more surface support points and prevent water droplets from penetrating recesses.

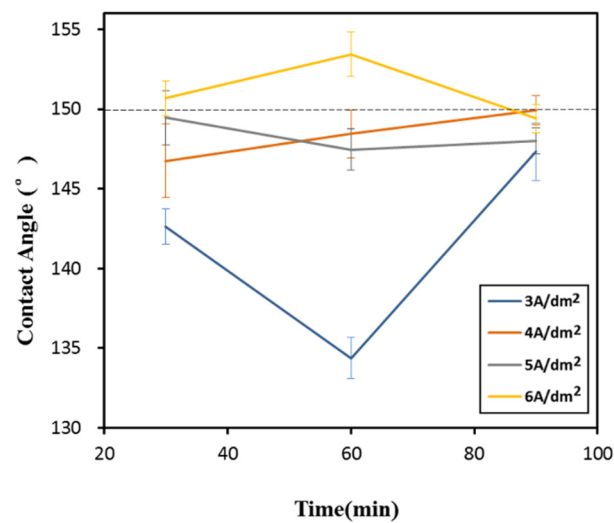


Figure 5. Plating time versus contact angle for the prepared samples.

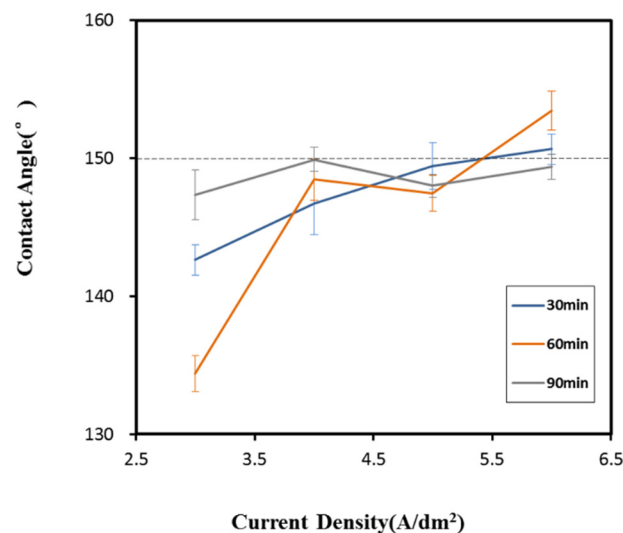


Figure 6. Plating current density versus contact angle for the prepared samples.

The effects of time and current density seem to be intricate. Here, taking a 6 A/dm² sample as an example, increasing deposition time increases the protrusion size. The growing protrusion leads to an increase in the specific surface area at the beginning. However, later, the increase in protrusion led to an increase in the percentage of solid–liquid contact area.

According to the Cassie–Baxter equation [41], increased r (corresponding to the specific surface area) leads to a large contact angle. Then, the decrease in f (corresponding to the percentage of the solid–liquid contact area) caused a slight contact angle.

$$\cos \theta = f(r \cos \theta_0 + 1) - 1 \quad (1)$$

Therefore, the time parameter for preparing superhydrophobic morphology needs to be coupled with the current density parameter. The above morphological and wettability analyses indicated that the contact angle of the sample obtained at a current density of 6 A/dm² and a time of 30 min exceeds 150°, which is the optimal preparation parameter for this process.

3.4. Superhydrophobic Surface Chemical Composition Analysis

In addition to surface morphology, chemical composition plays an important role in superhydrophobicity. In this section, we investigate the cause of superhydrophobicity in surface composition using a sample (60 min, 6 A/dm²).

Figure 7 depicts the XRD spectrum of the prepared superhydrophobic coating. The spectrum reveals that the crystalline phases present in the coating are mostly CuZn and Cu₅Zn₈, both of which are copper–zinc alloys. These copper–zinc alloys indicate the co-deposition of Cu²⁺ and Zn²⁺, resulting in the formation of a new phase. The XRD results also corroborate with the analysis of the chemical reaction process in the morphological analysis section. The detected iron phase is from the mild steel substrate.

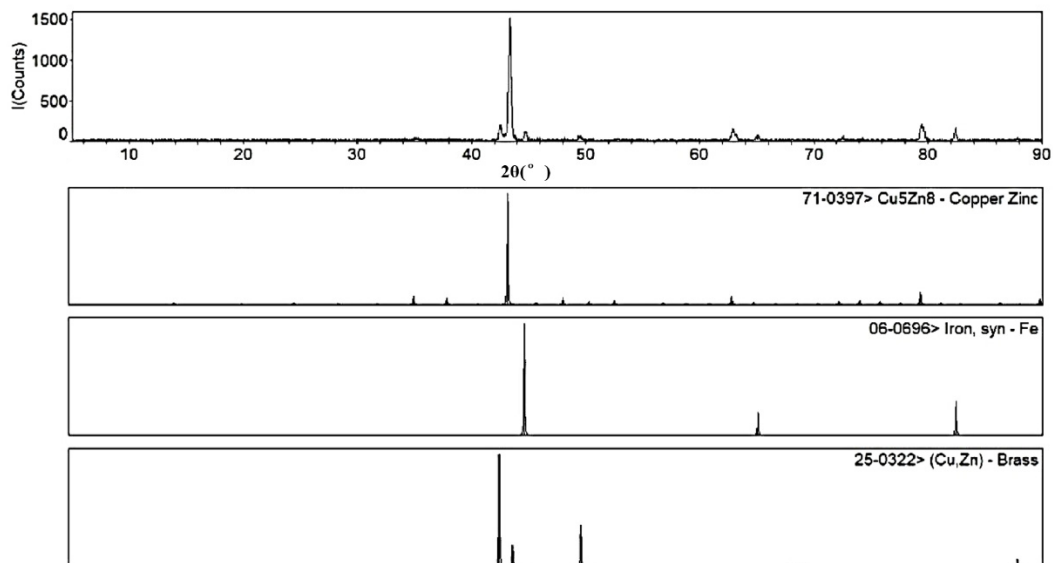


Figure 7. XRD spectrum of the prepared Cu-Zn superhydrophobic surfaces.

The EDS spectrum is shown in Figure 8 and the test results are listed in Table 2. The main elements of the coating are copper, zinc, and iron, which corroborate with the results of the XRD spectrum. In addition, a large amount of carbon was detected on the surface. The carbon element may come from the adsorption of hydrocarbons from the air. In order to confirm the present form of these elements on the surface, we performed an XPS analysis.

Table 2. Mass fraction and atomic percentage of the elemental content corresponding to EDS spectrum.

Elements	Weight	Atom
	%	%
C K	11.78	40.32
O K	1.56	4.02
Fe K	2.57	1.89
Cu K	48.10	31.13
Zn K	36.00	22.64
Total	100.00	

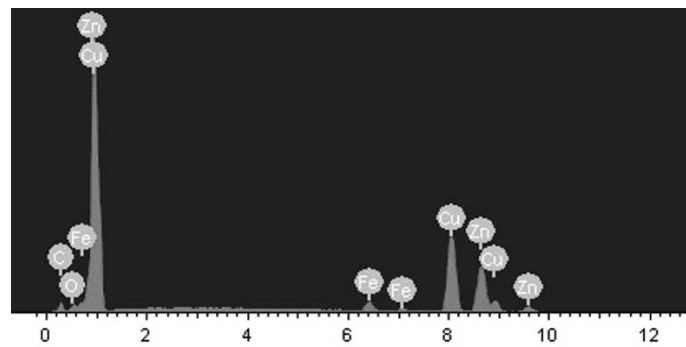


Figure 8. EDS spectrum of prepared Cu-Zn superhydrophobic surfaces.

The XPS spectrum (Figure 9) shows four main elements. They are Cu, Zn, O, and C and are consistent with previous XRD and EDS results. In Figure 10, the Cu 2p_{1/2} at 952.5 eV and Cu 2p_{3/2} peaks at 934.2 eV can be explained by the existence of Cu/Cu₂O and CuO. In Figure 11, the C 1s spectrum is disassembled into four peaks with binding energies of 284.5 eV, 286.6 eV, and 288.7 eV, 291.5 eV, and correspond to C-C/C=C, C-O, C=O, and -COO-, respectively. The hydrocarbons (C-H, C-C, and C=C) are in the majority. Figure 12 shows the O1s spectrum disassembled into two peaks at 531.1 eV and 532.5 eV from Cu₂O/ZnO and C-O species. In Figure 13, the Zn 2p_{3/2} at 1021.8 eV and the Zn 2p_{1/2} at 1044.8 eV correspond to the existence of ZnO. The elements of the prepared superhydrophobic surface, as well as their chemical state, were further examined by XPS. According to the chemical composition analysis, the electrodeposition method created a Cu-Zn composite layer on the mild steel substrate. After eight hours of heating in air at 200 degrees Celsius, the upper surface of the Cu-Zn coating developed copper oxides and zinc oxides. In accordance with previous research, we discovered that this transition metal oxide may spontaneously adsorb hydrocarbons in air, lowering the surface's energy. This conclusion was supported by the C1 spectrum of XPS. The absorbed airborne hydrocarbons combined with the micro/nano roughness caused the superhydrophobicity of the prepared mild steel-based Cu-Zn coating.

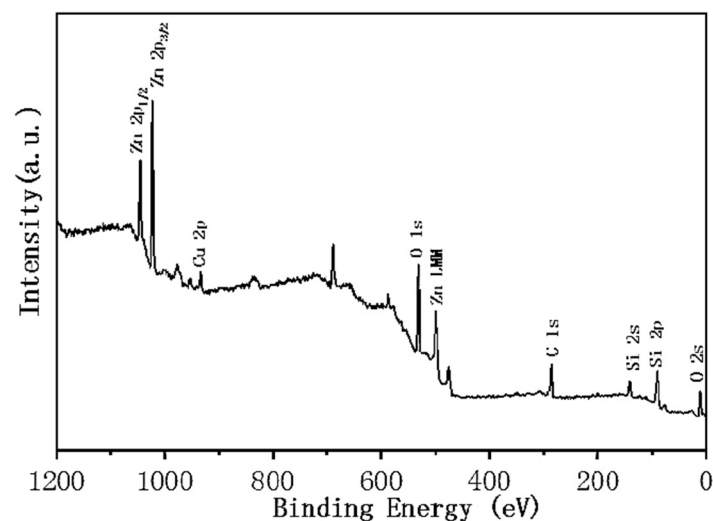


Figure 9. XPS spectrum shows four main elements: Cu, Zn, O, and C.

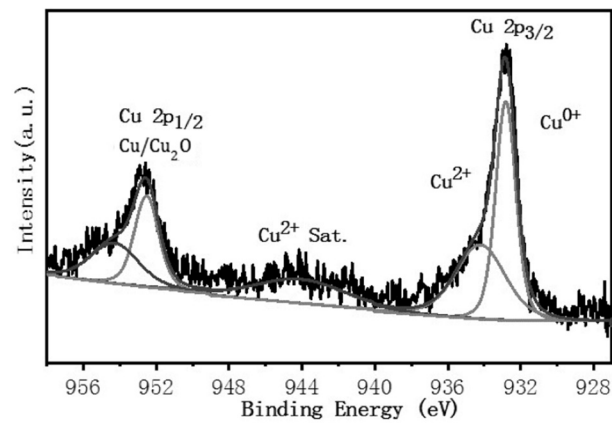


Figure 10. The Cu 2p_{1/2} at 952.5 eV and Cu 2p_{3/2} peaks at 934.2 eV can be explained by the existence of Cu/Cu₂O and CuO.

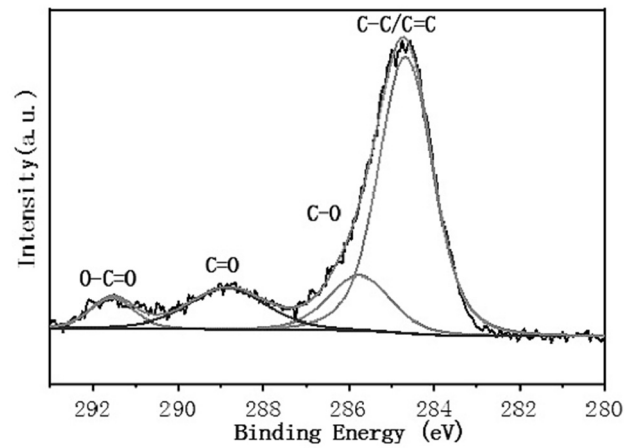


Figure 11. The C 1s spectrum: four peaks with binding energies of 284.5 eV, 286.6 eV and 288.7 eV, 291.5 eV.

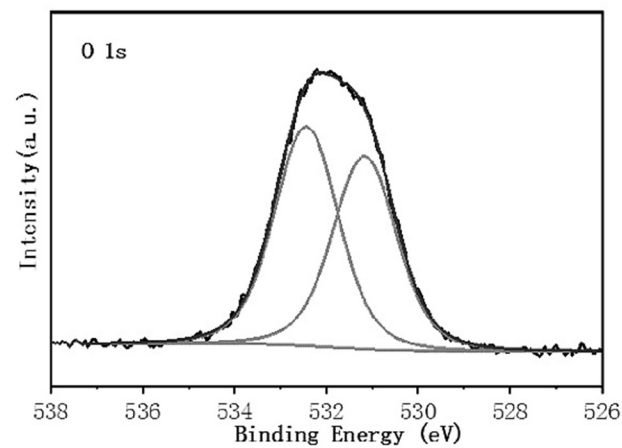


Figure 12. The O 1s spectrum disassembled into two peaks at 531.1 eV and 532.5 eV.

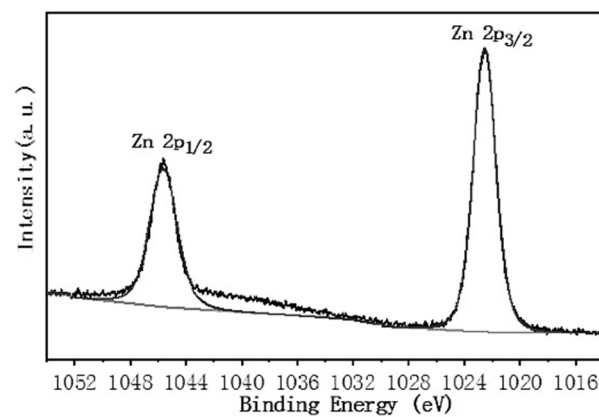


Figure 13. The Zn2p_{3/2} at 1021.8 eV and the Zn2p_{1/2} at 1044.8 eV correspond to the existence of ZnO.

3.5. Electrochemical Characterization

In order to analyze the corrosion resistance of the prepared Cu-Zn superhydrophobic surfaces, this study conducted AC (alternating current) impedance tests on the superhydrophobic surfaces in a 3.5% NaCl solution using an electrochemical workstation.

This test compared the mild steel plate, untreated Cu-Zn coating, and annealed superhydrophobic Cu-Zn coating. From the Nyquist plot (Figure 14a), it can be observed that the arc diameter of the superhydrophobic surface is larger than that of the untreated coating and the mild steel plate substrate, indicating that the prepared superhydrophobic surface has better corrosion resistance compared to the mild steel substrate. Moreover, this resistance improvement is not provided by the Cu-Zn coating. The Bode plots also confirm this conclusion (Figure 14b,c). The frequency–phase angle plot shows that the superhydrophobic surface corresponds to the highest phase angle, followed by the untreated coating and the steel plate on the frequency–impedance curve. It can be observed that the superhydrophobic surface also has the highest impedance modulus.

From the above analysis, it can be concluded that the superhydrophobic surface is more resistant to corrosion than the untreated Cu-Zn coating and mild steel substrate. Compared with the steel substrate, the untreated coating physically separates seawater from the steel substrate, impeding some seawater contact with the substrate. However, the surface voids and relatively high electrical conductivity still allow the corrosion process to occur slowly. After the annealing treatment, the Cu-Zn coating's contact angle increases, forming a discontinuous layer of air on the surface and forming a natural barrier that hinders ion transport and further retards the corrosion process [42].

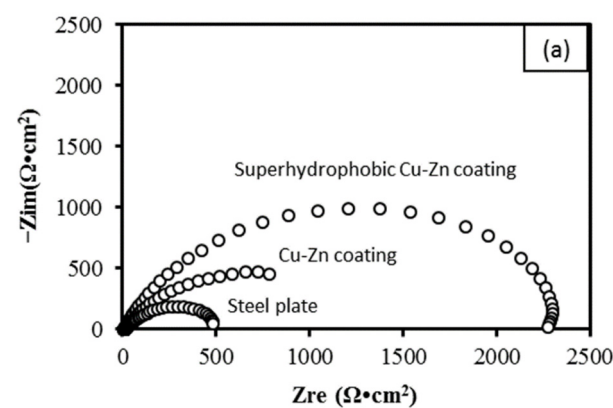


Figure 14. Cont.

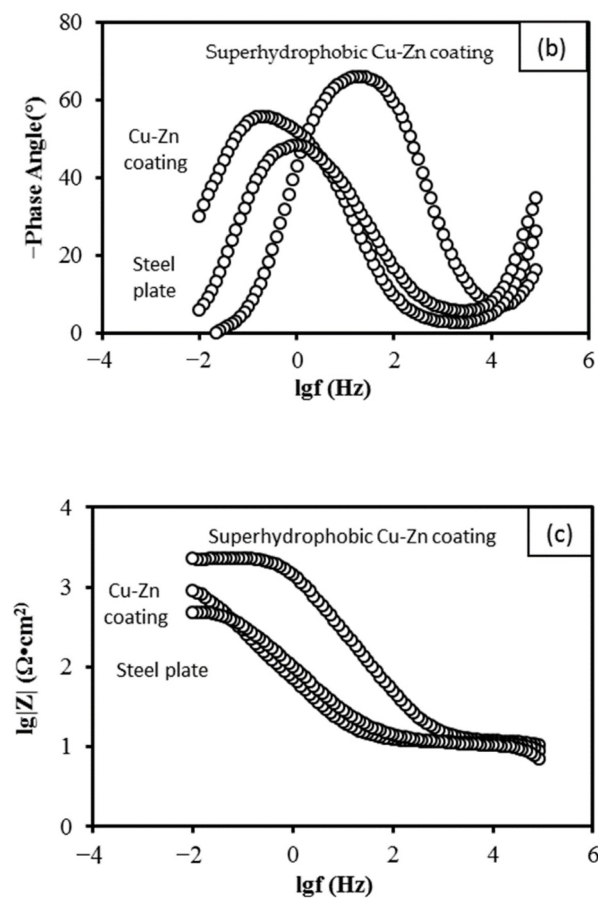


Figure 14. (a) the Nyquist plot (b,c) Bode plot of mild steel plate, untreated Cu-Zn coating, and annealed superhydrophobic Cu-Zn coating.

4. Conclusions

In this paper, a mild steel-based superhydrophobic coating was prepared using the Cu-Zn electrodeposition method followed by an annealing process. SEM images revealed numerous hierarchical micro/nanostructures on the surface. Current density values controlled the distribution density of the protrusions, and the size of each protrusion was controlled by deposition time. Both parameters contribute to the appropriate morphology to realize superhydrophobicity. The results of XPS, EDS, and XRD indicated the formation of copper oxide and zinc oxide. These two transition metal oxides spontaneously adsorb airborne hydrocarbons, contributing to low surface energy. Corrosion behavior in 3.5% NaCl solution was evaluated by EIS, which indicated improved corrosion resistance of the superhydrophobic surface compared to the untreated Cu-Zn coating and mild steel plate. The proposed method for preparing superhydrophobic coatings on mild steel surfaces is eco-friendly, safe, and simple and will have promising applications in the industry, especially in naval architecture and marine engineering.

Author Contributions: Conceptualization, W.J. and Y.L.; data curation, W.J.; formal analysis, W.J.; funding acquisition, J.W.; investigation, X.L.; methodology, W.J.; project administration, R.L.; resources, S.A.; supervision, Y.L.; validation, Y.L., J.W. and R.L.; visualization, X.L.; writing—original draft, W.J.; writing—review and editing, J.W. All authors have read and agreed to the published version of the manuscript.

Funding: This work was supported by the National Nature Science Foundation of China (Grant No.51479030).

Institutional Review Board Statement: Not applicable.

Informed Consent Statement: Not applicable.

Data Availability Statement: Not applicable.

Conflicts of Interest: The authors declare no conflict of interest.

References

1. Zhang, S.; Hou, L.; Du, H.; Wei, H.; Liu, B.; Wei, Y. A Study on the Interaction between Chloride Ions and CO₂ towards Carbon Steel Corrosion. *Corros. Sci.* **2020**, *167*, 108531. [[CrossRef](#)]
2. Wang, H.; Zhu, Y.; Hu, Z.; Zhang, X.; Wu, S.; Wang, R.; Zhu, Y. A Novel Electrodeposition Route for Fabrication of the Superhydrophobic Surface with Unique Self-Cleaning, Mechanical Abrasion and Corrosion Resistance Properties. *Chem. Eng. J.* **2016**, *303*, 37–47. [[CrossRef](#)]
3. Oguzie, E.E.; Enenebeaku, C.K.; Akalezi, C.O.; Okoro, S.C.; Ayuk, A.A.; Ejike, E.N. Adsorption and Corrosion-Inhibiting Effect of Daayodis Edulis Extract on Low-Carbon-Steel Corrosion in Acidic Media. *J. Colloid Interface Sci.* **2010**, *349*, 283–292. [[CrossRef](#)] [[PubMed](#)]
4. Tan, J.; Guo, L.; Yang, H.; Zhang, F.; El Bakri, Y. Synergistic Effect of Potassium Iodide and Sodium Dodecyl Sulfonate on the Corrosion Inhibition of Carbon Steel in HCl Medium: A Combined Experimental and Theoretical Investigation. *RSC Adv.* **2020**, *10*, 15163–15170. [[CrossRef](#)]
5. Hayatdavoudi, H.; Rahsepar, M. A Mechanistic Study of the Enhanced Cathodic Protection Performance of Graphene-Reinforced Zinc Rich Nanocomposite Coating for Corrosion Protection of Carbon Steel Substrate. *J. Alloys Compd.* **2017**, *727*, 1148–1156. [[CrossRef](#)]
6. Huang, J.; Lou, C.; Xu, D.; Lu, X.; Xin, Z.; Zhou, C. Cardanol-Based Polybenzoxazine Superhydrophobic Coating with Improved Corrosion Resistance on Mild Steel. *Prog. Org. Coat.* **2019**, *136*, 105191. [[CrossRef](#)]
7. Zhang, B.; Yan, J.; Xu, W.; Yu, T.; Chen, Z.; Duan, J. Eco-Friendly Anticorrosion Superhydrophobic Al₂O₃@PDMS Coating with Salt Deliquescence Self-Coalescence Behaviors Under High Atmospheric Humidity. *Front. Mater.* **2022**, *9*, 839948. [[CrossRef](#)]
8. Binyaseen, A.M.; Bayazeed, A.; Al-nami, S.Y.; Abu Al-Ola, K.; Alqarni, S.A.; Abdel-Hafez, S.H.; El-Metwaly, N.M. Development of Epoxy/Rice Straw-Based Cellulose Nanowhiskers Composite Smart Coating Immobilized with Rare-Earth Doped Aluminate: Photoluminescence and Anticorrosion Properties for Sustainability. *Ceram. Int.* **2022**, *48*, 4841–4850. [[CrossRef](#)]
9. Al-Qahtani, S.D.; Snari, R.M.; Alkhamis, K.; Alatawi, N.M.; Alhasani, M.; Al-Nami, S.Y.; El-Metwaly, N.M. Development of Silica-Coated Rare-Earth Doped Strontium Aluminate toward Superhydrophobic, Anti-Corrosive and Long-Persistent Photoluminescent Epoxy Coating. *Luminescence* **2022**, *37*, 479–489. [[CrossRef](#)]
10. Deng, X.; Mammen, L.; Zhao, Y.; Lellig, P.; Muellen, K.; Li, C.; Butt, H.-J.; Vollmer, D. Transparent, Thermally Stable and Mechanically Robust Superhydrophobic Surfaces Made from Porous Silica Capsules. *Adv. Mater.* **2011**, *23*, 2962–2965. [[CrossRef](#)]
11. Liu, H.; Wang, Y.; Huang, J.; Chen, Z.; Chen, G.; Lai, Y. Bioinspired Surfaces with Superamphiphobic Properties: Concepts, Synthesis, and Applications. *Adv. Funct. Mater.* **2018**, *28*, 1707415. [[CrossRef](#)]
12. Cao, X.; Pan, J.; Cai, G.; Xiao, S.; Ma, X.; Zhang, X.; Dong, Z. A Chemically Robust and Self-Healing Superhydrophobic Polybenzoxazine Coating without Fluorocarbon Resin Modification: Fabrication and Failure Mechanism. *Prog. Org. Coat.* **2022**, *163*, 106630. [[CrossRef](#)]
13. Lou, C.; Zhang, R.; Lu, X.; Zhou, C.; Xin, Z. Facile Fabrication of Epoxy/Polybenzoxazine Based Superhydrophobic Coating with Enhanced Corrosion Resistance and High Thermal Stability. *Colloids Surf. A Physicochem. Eng. Asp.* **2019**, *562*, 8–15. [[CrossRef](#)]
14. Vigdorovich, V.I.; Tsygankova, L.E.; Uryadnikova, M.N.; Emel'yanenko, K.A.; Chulkova, E.V.; Uryadnikov, A.A. Protective Effect of Superhydrophobic Coatings on Carbon Steel in Different Environments. *Int. J. Corros. Scale Inhib.* **2021**, *10*, 1157–1167. [[CrossRef](#)]
15. Tsygankova, L.E.; Vigdorovich, V.; Uryadnikov, A.A.; Vigdorowitsch, M.V.; Shel, E.Y.; Uryadnikova, M.N. Protection of Carbon Steel with Superhydrophobic Coating against Corrosion in NaCl Solution. *Surf. Interface Anal.* **2020**, *52*, 855–858. [[CrossRef](#)]
16. Cao, X.; Zhang, Y.; Hu, W.; Zheng, H.; Dan, Y.; Hu, J.; Chen, Z. Preparation of Superhydrophobic Nanoplate Iron Oxide Surface on a Carbon Steel for Anti-Wetting Applications. *Mater. Des.* **2021**, *211*, 110169. [[CrossRef](#)]
17. Bandi, P.; Muralidhar, K.V.; Kausley, S.; Rai, B. Development of Superhydrophobic and Corrosion Resistant Coatings on Mild Steel—A Greener Approach. *Mater. Today Commun.* **2020**, *25*, 101625. [[CrossRef](#)]
18. Du, C.; He, X.; Tian, F.; Bai, X.; Yuan, C. Preparation of Superhydrophobic Steel Surfaces with Chemical Stability and Corrosion. *Coatings* **2019**, *9*, 398. [[CrossRef](#)]
19. Leoni, G.B.; de Freitas, D.S.; Gomes, J.A.P.C.; Brasil, S.L.D.C. Evaluation of Structure, Heterogeneities, Thickness and Corrosion Protection of Electrodeposited Sol-Gel Superhydrophobic Coatings. *Mater. Res.* **2022**, *25*, e20210460. [[CrossRef](#)]
20. El-Din, M.R.N.; Hashem, A.; Morsi, R.E.; Abd El-Azeim, A. New Superhydrophobic Nanocomposites as Anti-Corrosion Coating Films. Part I: Synthesis and Characterization of Poly (Styrene/Vinyl Acetate)-SiO₂ Nanocomposites as a Water-Repelling Surface via Nanoemulsion Polymerization Technique. *J. Mol. Liq.* **2021**, *322*, 114885. [[CrossRef](#)]
21. Leoni, G.B.; de Freitas, D.S.; Ponciano Gomes, J.A.C.; Brasil, S.L.D.C. Multivariable Analysis of Electrodeposited Silane Based Superhydrophobic Coatings for Corrosion Protection of Carbon Steel. *J. Sol.-Gel. Sci. Technol.* **2020**, *94*, 695–707. [[CrossRef](#)]
22. Wang, S.; Xue, Y.; Ban, C.; Xue, Y.; Taleb, A.; Jin, Y. Fabrication of Robust Tungsten Carbide Particles Reinforced Co-Ni Superhydrophobic Composite Coating by Electrochemical Deposition. *Surf. Coat. Technol.* **2020**, *385*, 125390. [[CrossRef](#)]

23. Luo, S.; Zheng, L.; Luo, H.; Luo, C. A Ceramic Coating on Carbon Steel and Its Superhydrophobicity. *Appl. Surf. Sci.* **2019**, *486*, 371–375. [[CrossRef](#)]
24. Siddiqui, A.R.; Maurya, R.; Katiyar, P.K.; Balani, K. Superhydrophobic, Self-Cleaning Carbon Nanofiber CVD Coating for Corrosion Protection of AISI 1020 Steel and AZ31 Magnesium Alloys. *Surf. Coat. Technol.* **2020**, *404*, 126421. [[CrossRef](#)]
25. Wang, S.; Huang, H.; Li, X.; Yin, H.; Tang, J.; Hu, C.; Ma, B.; Li, T. An Effective Approach to Fabricate the Corrosion Resistance of Superhydrophobic ZnO/Ni Composite Coating on Carbon Steel Substrate. *J. Adhes. Sci. Technol.* **2021**, 1–18. [[CrossRef](#)]
26. Hu, C.; Xie, X.; Zheng, H.; Qing, Y.; Ren, K. Facile Fabrication of Superhydrophobic Zinc Coatings with Corrosion Resistance via an Electrodeposition Process. *New J. Chem.* **2020**, *44*, 8890–8901. [[CrossRef](#)]
27. Xue, Y.; Wang, S.; Zhao, G.; Taleb, A.; Jin, Y. Fabrication of Ni-Co Coating by Electrochemical Deposition with High Superhydrophobic Properties for Corrosion Protection. *Surf. Coat. Technol.* **2019**, *363*, 352–361. [[CrossRef](#)]
28. Xue, Y.; Wang, S.; Bi, P.; Zhao, G.; Jin, Y. Super-Hydrophobic Co-Ni Coating with High Abrasion Resistance Prepared by Electrodeposition. *Coatings* **2019**, *9*, 232. [[CrossRef](#)]
29. Hu, C.; Xie, X.; Ren, K. A Facile Method to Prepare Stearic Acid-TiO₂/Zinc Composite Coating with Multipronged Robustness, Self-Cleaning Property, and Corrosion Resistance. *J. Alloys Compd.* **2021**, *882*, 160636. [[CrossRef](#)]
30. Tian, G.; Zhang, M.; Zhao, Y.; Li, J.; Wang, H.; Zhang, X.; Yan, H. High Corrosion Protection Performance of a Novel Nonfluorinated Biomimetic Superhydrophobic Zn-Fe Coating with Echinopsis Multiplex-like Structure. *ACS Appl. Mater. Interfaces* **2019**, *11*, 38205–38217. [[CrossRef](#)]
31. Rasitha, T.P.; Vanithakumari, S.C.; George, R.P.; Philip, J. Template-Free One-Step Electrodeposition Method for Fabrication of Robust Superhydrophobic Coating on Ferritic Steel with Self-Cleaning Ability and Superior Corrosion Resistance. *Langmuir* **2019**, *35*, 12665–12679. [[CrossRef](#)]
32. Chen, C.; Fan, Y.; He, Y.; Chen, X.; Yang, Q. Fabrication of Superhydrophobic Zirconium Surface with a Facile Electrodeposition Process. *Surf. Innov.* **2018**, *6*, 106–115. [[CrossRef](#)]
33. Heidari, G.; Hosseini, S. Electrochemical Fabrication of Superhydrophobic and Superoleophilic Coating: Applications in Corrosion-Resistant Surfaces and Oil Cleanup. *Bull. Mater. Sci.* **2021**, *44*, 253. [[CrossRef](#)]
34. Prado, L.H.; Virtanen, S. Cu-MoS₂ Superhydrophobic Coating by Composite Electrodeposition. *Coatings* **2020**, *10*, 238. [[CrossRef](#)]
35. Wang, G.; Zhang, T.-Y. Oxygen Adsorption Induced Superhydrophilic-to-Superhydrophobic Transition on Hierarchical Nanostructured CuO Surface. *J. Colloid Interface Sci.* **2012**, *377*, 438–441. [[CrossRef](#)]
36. Liu, P.; Cao, L.; Zhao, W.; Xia, Y.; Huang, W.; Li, Z. Insights into the Superhydrophobicity of Metallic Surfaces Prepared by Electrodeposition Involving Spontaneous Adsorption of Airborne Hydrocarbons. *Appl. Surf. Sci.* **2015**, *324*, 576–583. [[CrossRef](#)]
37. Li, H.; Yu, S. Three-Level Hierarchical Superhydrophobic Cu-Zn Coating on a Steel Substrate without Chemical Modification for Self-Cleaning Property. *New J. Chem.* **2017**, *41*, 5436–5444. [[CrossRef](#)]
38. Darmanin, T.; de Givenchy, E.T.; Amigoni, S.; Guittard, F. Superhydrophobic Surfaces by Electrochemical Processes. *Adv. Mater.* **2013**, *25*, 1378–1394. [[CrossRef](#)]
39. Bordbar-Khiabani, A.; Yarmand, B.; Mozafari, M. Effect of ZnO Pore-Sealing Layer on Anti-Corrosion and in-Vitro Bioactivity Behavior of Plasma Electrolytic Oxidized AZ91 Magnesium Alloy. *Mater. Lett.* **2020**, *258*, 126779. [[CrossRef](#)]
40. Watanabe, T. *Nano-Plating: Microstructure Control Theory of Plated Film and Data Base of Plated Film Microstructure*; Elsevier Science: Amsterdam, The Netherlands, 2004; ISBN 978-0-08-044375-1.
41. Cassie, A.B.D.; Baxter, S. Wettability of Porous Surfaces. *Trans. Faraday Soc.* **1944**, *40*, 546–551. [[CrossRef](#)]
42. Jamali, R.; Bordbar-Khiabani, A.; Yarmand, B.; Mozafari, M.; Kolahi, A. Effects of Co-Incorporated Ternary Elements on Biocorrosion Stability, Antibacterial Efficacy, and Cytotoxicity of Plasma Electrolytic Oxidized Titanium for Implant Dentistry. *Mater. Chem. Phys.* **2022**, *276*, 125436. [[CrossRef](#)]